Title
Superconductivity in Nb-Sn Thin Films of Stoichiometric and Off-Stoichiometric Compositions

Journal
IEEE Transactions on Applied Superconductivity, 23(3)

ISSN
1051-8223

Authors
Mentink, MGT
Bonevich, JE
Dhalle, MMJ
et al.

Publication Date
2013

DOI
10.1109/tasc.2012.2235513

Peer reviewed

Superconductivity in Nb-Sn Thin Films of Stoichiometric and Off-Stoichiometric Compositions

M. G. T. Mentink, J. E. Bonevich, M. M. J. Dhalle, D. R. Dietderich, A. Godeke, F. Hellman, and H. H. J. ten Kate

***Abstract*—Binary Nb-Sn thin film samples were fabricated and characterized in terms of their composition, morphology, and superconducting properties. Nb-Sn was magnetron-sputtered onto heated R-plane sapphire substrates at 700 °C, 800 °C, and 900 °C, using a custom-built heater assembly. Samples were cut into strips, where each strip has a unique composition. For a subset of the samples, Nb-Sn was selectively etched away at an etching rate of 6 ± 1 nm/s using an aqueous solution of 3 vol.% hydrofluoric and 19 vol.% nitric acid. The sample composition was investigated with a scanning electron microscope with an X-ray energy dispersive spectroscopy detector. Surface and cross-section morphologies were investigated using scanning electron microscopy and scanning transmission electron microscopy, revealing a dense columnar poly-crystalline grain structure. X-ray diffraction measurements indicate a highly textured film that is (100) oriented out-of-plane and random in-plane. The critical temperature T_c (ranging from 9.8 to 17.9 K), critical magnetic field $\mu_0 H_{c2}$ (ranging from 12.5 to 31.3 T), residual resistivity ratio (RRR), and normal state resistivity ρ_0 were measured and found to be broadly consistent with literature data on bulk Nb_3Sn.**

***Index Terms*—Composition, morphology, Nb_3Sn, superconducting properties, thin film.**

I. Introduction

THE superconducting properties of Nb_3Sn, which is used for applications in which high magnetic field is required, such as the High Luminosity Large Hadron Collider, the International Thermonuclear Experimental Reactor, nuclear magnetic resonance magnets, and high field facilities, are strongly suppressed when the conductor is exposed to strain [1], affecting its performance in these applications.

This phenomenon is poorly understood and complicated by the fact that Nb_3Sn wires common for these applications contain Nb-Sn with various tin concentrations and grain sizes as well as additions such as titanium, tantalum and copper. To investigate how these various parameters affect the strain sensitivity of the wires, model samples with carefully controlled composition and morphology are required, see also [2].

In this article, the fabrication and characterization of binary Nb-Sn thin films with various tin concentrations is discussed in terms of composition, morphology, crystal orientation, superconducting properties, and normal state resistivity.

Manuscript received October 9, 2012; accepted December 17, 2012. Date of publication December 20, 2012; date of current version January 28, 2013. This work was supported in part by the Director, Office of Science, High Energy Physics (Godeke, Mentink, Dietderich), Basic Energy Sciences (Hellman), the U.S. Department of Energy under Contract DE-AC02-05CH11231.

M. G. T. Mentink is with the University of Twente, 7500AE Enschede, The Netherlands. He is also with the Lawrence Berkeley National Laboratory, Berkeley, CA 94720-8203 USA (e-mail: mgtmentink@lbl.gov).

J. E. Bonevich is with the National Institute of Standards and Technology, Gaithersburg, MD 20899 USA (e-mail: john.bonevich@nist.gov).

M. M. J. Dhalle and H. H. J. ten Kate are with the University of Twente, 7500AE Enschede, The Netherlands.

D. R. Dietderich and A. Godeke are with Lawrence Berkeley National Laboratory, Berkeley, CA 94720-8203 USA.

F. Hellman is with the Physics Department, University of California at Berkeley, Berkeley, CA 94704 USA (e-mail: fhellman@berkeley.edu).

Digital Object Identifier 10.1109/TASC.2012.2235513

II. Experiment

A. Sample Fabrication

Niobium and tin were magnetron sputtered simultaneously onto a heated R-plane sapphire substrate. A custom built PID-controlled heater was used, which consists of cartridge heaters and a K-type thermocouple inside a niobium block. Stainless steel heat shields reduce the power required to reach temperatures up to 1000 °C. Besides having a heater that closely matches the thermal expansion of sapphire [3] and Nb_3Sn [4], major advantages of this heater system include affordability, serviceability and durability. Thermal conductivity between the heater block and the substrate was enhanced with silver paint, which was briefly heated up to 150 °C in atmosphere. The substrate was cleaned with acetone, iso-propanol and electronic grade iso-propanol in an ultrasonic bath. After cleaning and mounting on the heater, the substrate was held in place with a molybdenum clip.

Before deposition, the chamber was pumped down and heated until the base pressure was sufficiently low. The achieved base pressures of the depositions at 700, 800, and 900 °C were 4.7×10^{-6}, 9.9×10^{-6} and 1.6×10^{-5} Pa, respectively. Argon gas was then introduced into the chamber and regulated at a pressure of 0.27 Pa. Niobium was sputtered onto the shutter for several minutes to getter gaseous contaminants. After the acceleration voltage of the guns had stabilized, typically at 250 W (355 V) and 40 W (570 V) for the niobium and tin target respectively, the shutter was opened. Deposition occurred at a typical effective rate of 0.32 nm/s. After the deposition was completed and the sample had cooled down in vacuum, the sample was cut into strips that are typically 1–4 mm wide and 25.4 mm long.

B. Etching

A limited subset of the samples was patterned to enable simultaneous measurement of the superconducting and normal state properties as a function of longitudinal and transverse strain, and to allow for critical current measurements and resistivity measurements in a well-defined geometry.

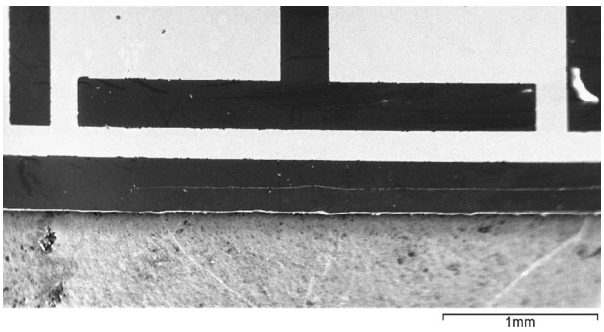

Fig. 1. Surface image of a selectively etched Nb-Sn thin film. The bright regions are the Nb-Sn layer, while the dark regions are the exposed sapphire substrate.

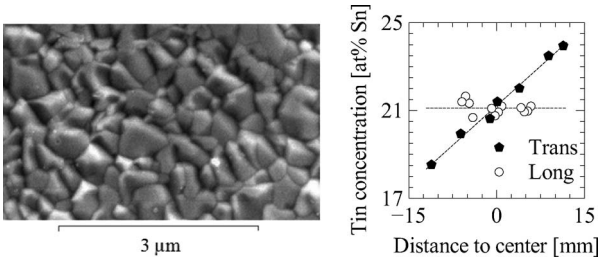

Fig. 2. Surface image (left) and composition along longitudinal and transverse direction (right) of a Nb-Sn thin film that was deposited at 900 °C. The lines are guides to the eye.

To pattern the films, an aqueous solution [5] of 7 vol.% hydrofluoric acid, 43 vol.% nitric acid and 50 vol.% distilled water was repeatedly diluted with distilled water and tested, until a suitable mixture of 3 vol.% hydrofluoric acid and 19 vol.% nitric acid was found, which etches through the Nb-Sn layer at a controlled rate of 6 ± 1 nm/s.

A positive photo-resist layer was spun onto a sample, and the areas where etching is desired were exposed to 12.5 mW/cm^2 of ultra-violet light for 12.5 s. After the exposed photo-resist was dissolved with a developer, the sample was baked at 120 °C for 30 minutes. Finally the sample was placed in the etching solution and the exposed Nb-Sn layer was fully etched through in approximately 6 minutes, see Fig. 1.

C. Morphology: SEM Surface Image and STEM Cross-Section

SEM and STEM techniques were used to investigate the morphology of the Nb-Sn thin films. A poly-crystalline grain structure was observed, see left side of Fig. 2. Typical grains vary in size between 100 nm and 1 μm, with an average size of about 300 nm. A STEM image made with a high angle annular dark field detector (HAADF) shows a dense film with columnar grains and a thickness of 2.3 μm, see Fig. 3.

D. Composition: SEM-XEDS Analysis

The composition of each of the strips was determined using SEM-XEDS. The measured tin content along the length of each of the strips is constant, within an uncertainty of 0.5 at.% Sn, see right side of Fig. 2. It should be noted that this technique measures an average composition with a typical probing volume of 1.5 μm^3, so inhomogeneity on a smaller scale is (partially) averaged out.

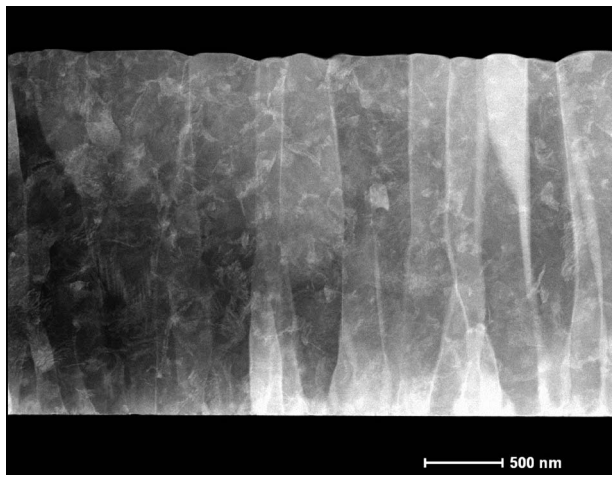

Fig. 3. Cross-section of a Nb-Sn thin film that was deposited at 900 °C.

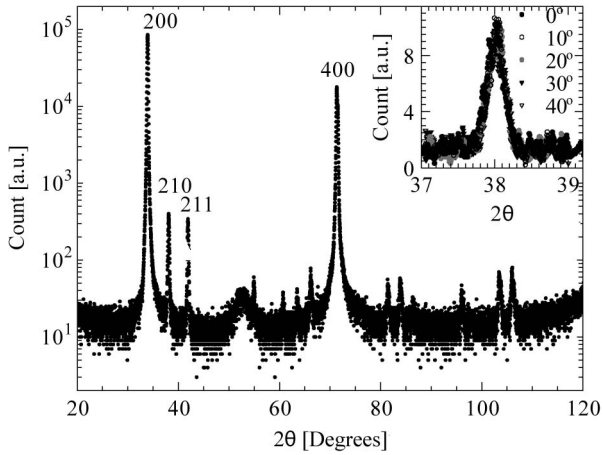

Fig. 4. $\theta - 2\theta$ scan of the Nb-Sn thin film that was deposited at 800 °C, with a full width at half maximum of 0.2 degrees in the (200) peak. Inset: The (210) off-axis peak corresponding to the (200) out-of-plane peak.

In the transverse direction, a typical range of 5 to 6 at.% Sn was observed per deposition, thus one deposition covers most of the stable Nb-Sn composition range [6]. Consistent with literature, see [7], tin concentrations above approximately 25 at.% Sn were not observed in the samples deposited at 800 °C or above, while in the sample deposited at 700 °C the excess Sn is contained in a Nb_6Sn_5 phase.

E. Crystal Orientation: X-Ray Diffraction Measurement

The crystal orientation of the samples was investigated with a standard $\theta - 2\theta$ scan to determine the out-of-plane orientation, and an off-axis scan at various rotations to determine the in-plane orientation. The $\theta - 2\theta$ scan indicates that the samples are highly textured and preferably oriented (100) out-of-plane, with a (200) to (210) peak ratio of 20, 213 and 13 for the samples deposited at 700, 800 and 900 °C, respectively, see Fig. 4. For comparison, the (200) to (210) ratio in a sample with randomly oriented Nb_3Sn grains is 0.45/1 [8].

Using a 4-circle diffractometer, the sample was tilted 26.56 degrees to the side, such that the (210) off-axis peak corresponding to the (100) out-of-plane crystal orientation was found. The relationship between sample rotation about the

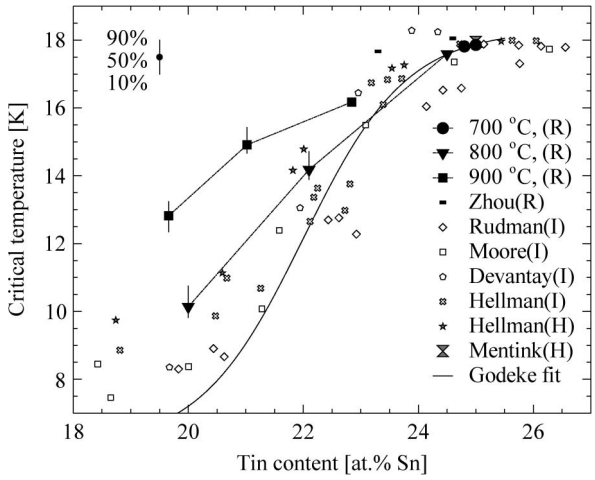

Fig. 5. T_c as a function of composition, compared to resistive (R), inductive (I) and heat capacity (H) measurements on various bulk samples and thin films from literature. For the inductive and heat capacity measurements, the onset temperature is used [2], [7], [11], [12], [17], [19]. The fit is a summary of the average critical temperature of bulk samples [15]. The vertical lines indicate the width of the T_c distribution.

surface normal and intensity of the (210) off-axis peak was then investigated by repeatedly performing $\theta - 2\theta$ scans for various sample rotation angles. The intensity of the (210) peak is independent of sample rotation, a clear indication that the in-plane orientation of the sample is random, see Fig. 4, inset.

F. Cryogenic Measurements of $R(T, B)$

Cryogenic measurements were performed, by which the resistance was measured as a function of temperature, magnetic field, strain, and current. This article focuses on the measurements of resistance as a function of temperature and magnetic field, without applying strain. The measurement setup [1] was optimized [9] and validated [10] for the purpose of investigating bulk samples and thin films. Four point probe measurements of resistance were performed with a measuring current of 10 μA, and for each sample it was verified that the magnitude of this current on the superconducting properties is negligible. Voltage and current leads were connected to the sample with silver paint, making sure that the distance between the leads was at least several millimeters.

III. Results and Data Reduction

Analogous to previous work [2], the critical temperature T_c for a given magnetic field was determined using a resistance criterion, see Fig. 5, and compared to literature results [2], [7], [11], [12], [17], [19]. The $T_c(\mu_0 H \geq 5\,\mathrm{T})$ data were fitted using the Maki-De Gennes equation [13], [14], see Fig. 6, to find an extrapolated H_{c2}, see Fig. 7. The extrapolated T_c is consistently 0.2 to 0.6 K lower than the measured T_c, see Fig. 6. Besides the measured T_c and extrapolated H_{c2}, ρ_0, see Fig. 8, and RRR are listed in Table I.

IV. Discussion

Resistive measurements of the critical temperature preferentially probe the composition with highest critical temperature in

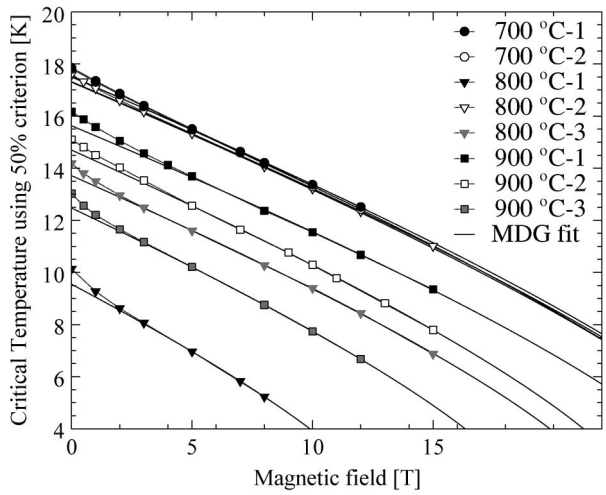

Fig. 6. Critical temperature as a function of magnetic field for the various samples, compared to Maki-De Gennes fits.

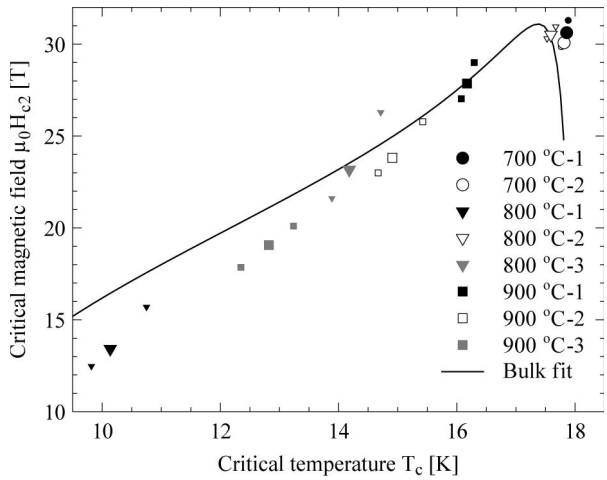

Fig. 7. Relationship between measured T_c and extrapolated H_{c2} of the thin films, compared to an analytical summary of binary Nb-Sn bulk samples [15]. The large symbols indicate superconducting properties that are determined using a 50% resistance criterion, while for the smaller symbols, 10% and 90% resistance criteria are used.

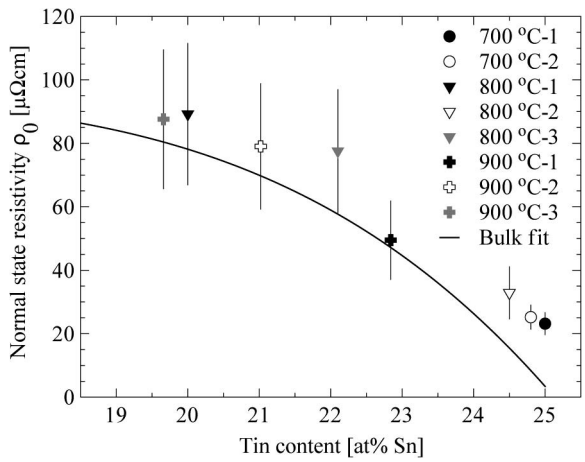

Fig. 8. Normal state resistivity as a function of sample composition, compared to an analytical summary of binary Nb-Sn bulk samples [15], also see [16]. The uncertainty in ρ_0 is due to uncertainty in geometry.

TABLE I
SUPERCONDUCTING AND NORMAL STATE PROPERTIES

	700 °C-1	700 °C-2	800 °C-1	800 °C-2
Tin content [at.% Sn]	25.0	24.8	20.0	24.5
$T_{c,10\%}$ [K]	17.8	17.9	9.8	17.5
$T_{c,50\%}$ [K]	17.9	17.8	10.1	17.6
$T_{c,90\%}$ [K]	17.9	17.9	10.8	17.7
$T_{c,90\%}$-$T_{c,10\%}$ [K]	0.04	0.09	0.93	0.15
$\mu_0 H_{c2,10\%}$ [T]	30.2	29.9	12.5	30.3
$\mu_0 H_{c2,50\%}$ [T]	30.6	30.1	13.4	30.5
$\mu_0 H_{c2,90\%}$ [T]	31.3	30.7	15.7	30.9
ρ_0 [$\mu\Omega$cm]	23	25	89	33
RRR	3.87	3.46	1.25	3.14
	800 °C-3	900 °C-1	900 °C-2	900 °C-3
Tin content [at.% Sn]	22.1	22.8	21.0	19.7
$T_{c,10\%}$ [K]	13.9	16.1	14.7	12.4
$T_{c,50\%}$ [K]	14.2	16.2	14.9	12.8
$T_{c,90\%}$ [K]	14.7	16.3	15.4	13.2
$T_{c,90\%}$-$T_{c,10\%}$ [K]	0.83	0.22	0.75	0.89
$\mu_0 H_{c2,10\%}$ [T]	21.6	27.0	23.0	17.9
$\mu_0 H_{c2,50\%}$ [T]	23.2	27.9	23.8	19.1
$\mu_0 H_{c2,90\%}$ [T]	26.3	29.0	25.8	20.1
ρ_0 [$\mu\Omega$cm]	78	49	79	88
RRR	1.53	1.88	1.43	1.27

a sample, as only a fraction of the sample needs to be superconducting to form a superconducting path. This implies that the actual critical temperature distribution in each of the resistively measured samples is broader than the resistively observed critical temperature distribution. Heat capacity measurements, the most reliable method for probing the volumetric critical temperature distribution, show that thoroughly optimized off-stoichiometric Nb-Sn thin films have critical temperature distributions that are typically several Kelvin wide [17]. This is in stark contrast to the samples with compositions near stoichiometry where the observed critical temperature distribution is as little as 0.04 Kelvin wide, see Table I.

While the critical temperature distributions of the samples that were deposited at 800 °C are consistent with literature, some of the critical temperature distributions of the samples that were deposited at 900 °C are relatively high. In previous Nb-Sn thin film work [17], a model was developed that relates the local variation in tin content to variation in crystal orientation relative to the surface. Thus, samples with a lower degree of texturing are expected to be less homogeneous in composition, which would result in the observed higher critical temperature [17], see Section II-E.

Another possibility is that the critical temperature is affected by the presence of oxygen during the deposition. Such an effect was demonstrated in Nb-Sn depositions, deposited at a four times higher deposition rate with partial oxygen pressures of 6.7×10^{-5} to 1.3×10^{-4} Pa [17]. This could imply that during the deposition some of the niobium is trapped as Nb-O, reducing the niobium available for Nb-Sn formation. While these partial oxygen pressures are significantly above the base pressure at which our samples were deposited and the oxygen content of the argon is only 2×10^{-5} at.%, the observed effect on the critical temperature is very similar.

In all samples, a distinct upward curve in the critical temperature is observed at magnetic fields close to 0 T, something that has previously been observed for stoichiometric samples [10], [18]–[20]. Two possible explanations for this phenomenon are expressed in terms of anisotropy of the Fermi surface [21], [22], and the existence of a second gap [20].

The relationship between critical temperature and critical magnetic field is very close to the literature result [15], see Fig. 7. Nb-Sn with a higher critical temperature generally has a higher critical magnetic field [15]. When taking compositional inhomogeneity into account, the same fraction of the sample always dominates the normal to superconducting state transition, independent of magnetic field. While a drop in the critical magnetic field is expected near stoichiometry, it is likely that the Nb-Sn with slightly lower tin concentration and higher critical magnetic field dominates over the stoichiometric Nb_3Sn with lower critical magnetic field in our samples.

Finally the normal state resistivity of the samples near stoichiometry is higher than expected [15]. Possible explanations for this are impurity and defect scattering.

V. CONCLUSION

Binary stoichiometric and off-stoichiometric Nb-Sn thin films were fabricated by simultaneously depositing niobium and tin onto a sapphire substrate, that was heated to 700, 800, or 900 °C. A novel heater system was developed and discussed in terms of ease of use, durability and affordability.

The films are shown to be poly-crystalline, consisting of dense columnar grains, as well as macroscopically homogeneous in tin content within an uncertainty of 0.5 at.% Sn. X-ray diffraction measurements show that the films are highly textured and oriented (100) out-of-plane and random in-plane.

The critical temperature, critical magnetic field, normal state resistivity, and residual resistivity ratio were determined using a technique in which resistance is measured as a function of magnetic field and temperature. Critical temperatures between 9.8 and 17.9 K and critical magnetic fields between 12.5 and 31.3 T were found.

Deviations of the expected critical temperature are observed in some of the samples, and possible explanations are discussed.

Fabricating and fully characterizing stoichiometric and off-stoichiometric Nb-Sn is an important step towards mapping the relationship between composition and strain sensitivity in Nb_3Sn.

ACKNOWLEDGMENT

The authors thank J. Slack (LBNL) and F. Roesthuis (UT) for their advice on thin film deposition.

REFERENCES

[1] B. ten Haken, A. Godeke, and H. H. J. ten Kate, "The strain dependence of the critical properties of Nb_3Sn conductors," *J. Appl. Phys.*, vol. 85, no. 6, pp. 3247–3253, 1999.

[2] M. G. T. Mentink, M. M. J. Dhalle, D. R. Dietderich, A. Godeke, W. Goldacker, F. Hellman, M. D. Sumption, M. A. Susner, and H. H. J. ten Kate, "The effect of Ta and Ti additions on the strain sensitivity of bulk niobium-tin," *Phys. Proc.*, vol. 35, pp. 491–496, 2012.

[3] W. M. Yim and R. J. Paff, "Thermal expansion of AlN, sapphire, and silicon," *J. Appl. Phys.*, vol. 45, no. 3, pp. 1456–1457, 1974.

[4] Y. S. Touloukian, R. K. Kirby, R. E. Taylor, and P. D. Desai, *Thermophysical Properties of Matter*. New York: Plenum, 1975, ISBN 0-306-67032-1, Table 126R.
[5] G. F. Vander Voort, *Metallography, Principles and Practise*, 1984, p. 670, ISBN-10: 0871706725.
[6] J. P. Charlesworth, I. Macphail, and P. E. Madsen, "Experimental work on the Niobium-Tin consitution diagram and related studies," *J. Mater. Sci*, vol. 5, pp. 580–603, 1970.
[7] D. A. Rudman, F. Hellman, R. H. Hammond, and M. R. Beasley, "A15 Nb-Sn tunnel junction fabrication and properties," *J. Appl. Phys.*, vol. 55, no. 10, pp. 3544–3553, 1984.
[8] G. W. Cullen, *Trans. Met. Soc. AIME 230*, vol. 1494, 1964.
[9] M. G. T. Mentink, A. Anders, M. M. J. Dhalle, D. R. Dietderich, A. Godeke, W. Goldacker, F. Hellman, H. H. J. ten Kate, D. Putnam, J. L. Slack, M. D. Sumption, and M. A. Susner, "Analysis of bulk and thin film model samples intended for investigating the strain sensitivity of niobium-tin," *IEEE Trans. Appl. Supercond.*, vol. 21, no. 3, pp. 2550–2553, Jun. 2011.
[10] M. G. T. Mentink, M. M. J. Dhalle, D. R. Dietderich, A. Godeke, W. Goldacker, F. Hellman, and H. H. J. ten Kate, "Towards analysis of the electron density of states of Nb_3Sn as a function of strain," *Adv. Cryog. Eng.*, vol. 58, pp. 225–232, 2012.
[11] J. Zhou, Y. Jo, Z. H. Sung, H. Zhou, P. J. Lee, and D. C. Larbalestier, "Evidence that the upper critical field of Nb_3Sn is independent of whether it is cubic or tetragonal," *Appl. Phys. Lett.*, vol. 99, p. 122 507, 2011.
[12] D. F. Moore, R. B. Zubeck, and J. M. Rowell, "Energy gaps of the A-15 superconductors Nb_3Sn, V_3Si, and Nb_3Ge measured by tunneling," *Phys. Rev. B, Condens. Matter*, vol. 20, no. 7, pp. 2721–2738, 1979.
[13] P. G. De Gennes, *Superconductivity of Metals and Alloys*. Orsay, France, 1966.
[14] A. Godeke, M. C. Jewell, C. M. Fischer, A. A. Squitieri, P. J. Lee, and D. C. Larbalestier, "The upper critical field of filamentary Nb_3Sn conductors," *J. Appl. Phys.*, vol. 97, p. 093909, 2005.
[15] A. Godeke, "A review of the properties of Nb_3Sn and their variation with A15 composition, morphology and strain state," *Supercond. Sci. Technol.*, vol. 19, pp. R68–R80, 2006.
[16] R. Flukiger, D. Uglietti, C. Senatore, and F. Buta, "Microstructure, composition and critical current density of superconducting Nb_3Sn wires," *Cryogenics*, vol. 48, pp. 293–307, 2008.
[17] F. Hellman, "Specific heat and non-equilibrium aspects of vapor deposition growth of A15 superconductors," Ph.D. dissertation, Stanford Univ., Stanford, CA, 1985.
[18] T. P. Orlando, E. J. McNiff, S. Foner, and M. R. Beasley, "Critical fields, Pauli paramagnetic limiting, and material properties of Nb_3Sn and V_3Si," *Phys. Rev. B, Condens. Matter Mater. Phys.*, vol. 19, pp. 4545–4561, 1979.
[19] H. Devantay, J. L. Jorda, M. Decroux, and J. Muller, "The physical and structural properties of superconducting A15-type Nb-Sn alloys," *J. Mater. Sci.*, vol. 16, pp. 2145–2153, 1981.
[20] V. Guritanu, W. Goldacker, F. Bouquet, Y. Wang, R. Lortz, G. Goll, and A. Junod, "Specific heat of Nb_3Sn: The case for a second energy gap," *Phys. Rev.B.*, vol. 70, p. 184 526, 2004.
[21] N. R. Werthamer and W. L. McMillan, "Temperature and purity dependence of the superconducting critical field H_c2. IV. Strong-coupling effects," *Phys. Rev.*, vol. 158, no. 2, pp. 415–417, 1967.
[22] E. Schachinger and M. Prohammer, "Anisotropy effects in the A15 superconductor Nb_3Sn," *Phys. C*, vol. 156, pp. 701–706, 1988.